Synergistic coupling of CoFe-LDH arrays with NiFe-LDH nanosheet for highly efficient overall water splitting in alkaline media

Rong Yang[a], Yimeng Zhou[a], Yingying Xing[b], Di Li[b,*], Deli Jiang[a], Min Chen[a], Weidong Shi[a,*], Shouqi Yuan[b]

[a] School of Chemistry and Chemical Engineering, Jiangsu University, Zhenjiang, 212013, China
[b] Institute for Energy Research, Jiangsu University, Zhenjiang, 212013, China

ARTICLE INFO

ABSTRACT

Developing active, stable and cost-effective bifunctional electrocatalysts with earth-abundant metals (Ni, Fe, Co) is a prerequisite to achieve overall water splitting. In this work, a novel CoFe-layered double hydroxide (LDH) coupled with NiFe-LDH nanosheet array supported on nickel foam (denoted as CoFe@NiFe/NF) is developed through a facile hydrothermal and electrodeposition method. Remarkably, benefiting from strong synergistic effect between CoFe-LDH and NiFe-LDH and the unique structural features, the resulting CoFe@NiFe/NF architectures catalyst exhibits excellent activities and stabilities for oxygen evolution reaction (OER) and hydrogen evolution reaction (HER). Furthermore, an efficient and stable alkali-electrolyzer using CoFe@NiFe/NF as both the cathode and anode achieve a voltage of $1.59\,V$ at the current density of $10\,mA\,cm^{-2}$, which is superior to many other state-of-the-art earth-abundant electrocatalysts. This work provides a facile method for enhancing the electrocatalytic activity by constructing hierarchical core-shell architectures using the LDH nanosheet materials.

1. Introduction

Nowadays, exploring clean and sustainable energy sources is of great important for the alleviation of the current energy crisis. Hydrogen is one of the most ideal candidates owing to its excellent energy density and zero pollution [1–5]. Among multiple methods, hydrogen produced electrochemical water splitting involving two important reactions including hydrogen evolution reaction (HER) and oxygen evolution reaction (OER) is considered as an effective strategy [6–10]. So far, noble-metal like Pt-based and Ir-based catalysts has been identified as benchmark HER and OER electrocatalysts, respectively. However, the cost and scarcity of these noble-metal catalysts tremendously limit their widespread application [11–14]. Thus, the development of an efficient and nonprecious electrocatalyst based on earth abundant elements are highly required [15,16]. Although rapid advances have been made, most electrocatalysts are only active towards either HER or OER, owing to the incompatibility of the stability and activity of HER and OER catalysts in the same electrolyte media. In practical production, numerous water splitting electrolyzers only work well under alkaline condition [17–19]. Therefore, it is a laborious task to seek effective bifunctional catalysts for simultaneously catalyzing

HER and OER under the same condition especially in alkaline condition [20–22].

To meet the challenges, researches emphasized that transition metal-based compounds hold an efficient and promising status to supersede noble metal catalysts [23–27]. Layered double hydroxides (LDHs) have emerged as a new class of promising nonprecious bifunctional electrocatalysts in alkaline electrolyte solutions owing to its special 2D structure with large surface areas, tunable compositions, and earth abundance [28–30]. In particular, recent studies demonstrated that CoFe-based LDHs holds a great promise as a water splitting electrocatalyst due to the strong synergistic effect between Co and Fe ions [31]. Notwithstanding, the performance of CoFe-based LDHs is still limited by its low electrical conductivity and sluggish water dissociation process [32]. To improve the catalytic efficiency of LDHs-based electrocatalysts, several feasible strategies have been proposed, such as nanostructuring to increase the active surface area, electronic structure modulation and hybridization to accelerate the charge transfer and optimize the binding energies between the catalyst and the reaction intermediates [33–38]. Among them, construction of interface engineered core-shell architectures consisting of two or more active components received more attentions. The hierarchical architectures

---

featuring enlarged surface area can provide more active sites, which is also very significant for both HER and OER. Importantly, the created nanointerfaces between the coupling materials can facilitate the charge transfer and provide more opportunities in tuning the adsorption-desorption energies, therefore further accelerating the hydrogen evolution reactions. The previously reported LDH-based electrocatalysts normally showed moderate or high OER activity due to its proper oxygen binding energies. In contrast, the HER activity of these LDH-based electrocatalysts was less studied, possible due to the large overpotential and/or instability of LDH in acidic media. As a typical LDHs material, NiFe-LDH nanosheets catalyst has been regarded as one of the most effective catalysts in alkaline electrolyte and was easy to construct hybrid electrocatalysts with enhanced OER and HER activities [39–44]. For instances, Jiang and co-workers engineered the $NiCo_2S_4$@NiFe LDH heterostructure interface and obtained significantly enhanced HER and OER activities mainly due to the strong interaction and charge transfer between $NiCo_2S_4$ nanowire core and NiFe-LDH nanosheet shell [45]. Zhou et al. constructed CoNiP@NiFe-LDH hierarchical arrays which exhibited outstanding electrocatalytic activity and long-term durability due to the synergetic effects of the CoNiP core and NiFe-LDH shell [46]. Recently, Yang and co-workers constructed MoS_2/NiCo-LDH hybrid electrocatalyst and demonstrated the synergistic effect of MoS_2 (as a hydrogen acceptor) and LDHs (as a hydroxyl acceptor) in promotion of the H_2O dissociation in alkaline media, which accounts for the significant enhanced HER activity [33]. Considering the strong binding strength to hydroxyl of LDHs favorable for the dissociation of H_2O as well as the 2D nanosheet structure with large surface area and the advantages of hierarchical core-shell architectures, integration of CoFe-LDH with NiFe-LDH will be an effective means to obtain a novel efficient electrocatalyst toward overall water splitting in an alkaline electrolyte.

Encouraged by these considerations, in this work, we reported the design and manufacture of an integrated 3D hierarchical CoFe-LDH@NiFe-LDH core-shell architectures supported on nickel foam (denoted as CoFe@NiFe/NF) through in-situ electrochemically assembling NiFe-LDH on the CoFe-LDH nanosheet arrays. As expected, this CoFe@NiFe/NF architecture electrocatalyst exhibited efficient bifunctional performance with low overpotentials of 160 mV and 240 mV toward OER and HER in an alkaline solution at the current density of 10 mV cm^{-2}, respectively. Remarkably, the symmetrical two-electrode cell using CoFe@NiFe/NF as both the cathode and anode acquire only 1.59 V at the current density of 10 mA cm^{-2}, which outperformed many other state-of-the-art overall water-splitting electrocatalysts. Given the high electrocatalytic activity and stability, together with its low cost and natural abundance of LDHs materials, it is expected that the present CoFe@NiFe/NF electrocatalyst hold great promise in the practical alkaline overall water splitting.

2. Experimental sections

2.1. Materials

All the chemicals were of analytical grade and used directly without any further purification after purchasing. Cobalt (II) nitrate hexahydrate ($Co(NO_3)_2$·6H_2O), Ferrous (III) nitrate hexahydrate (Fe$(NO_3)_3$·9H_2O), urea ($CO(NH_2)_2$), ammonium fluoride(NH_4F), Nickel (II) nitrate hexahydrate ($Ni(NO_3)_2$·6H_2O), Iron (II) sulfate heptahydrate, potassium hydroxide (KOH), hydrochloric acid (HCl), sulfuric acid (H_2SO_4), absolute ethanol and acetone were purchased from Sinopharm Chemical Reagent Co., Ltd (Shanghai, China). Iridium powder (Ir/C, 5 wt%) and platinum carbon powder (Pt/C, 20 wt%) were commercial products obtained from Aladdin (Shanghai, China). Nafion solution (5 wt%) was bought from Dupont China Holding Co., Ltd (Tianjin, China). NF with a thickness of 1.6 mm and 120 ppi (pore per square inch) was purchased from Jia Shide Foam Metal Co., Ltd (Suzhou, China). Deionized water was used throughout the experiments.

2.2. Synthesis of CoFe-LDH/NF nanoarrays

Previous to the synthesis, a piece of Ni foam (NF) was first dipped in diluted hydrochloric acid to remove the oxide films on the surface, followed by sonication in acetone for 15 min and finally cleaned by ethanol and deionized water for several times before use. In a typical process, 0.5 mmol of Fe$(NO_3)_3$·9H_2O, 0.5 mmol of $Co(NO_3)_2$·6H_2O, 10 mmol of urea and 4 mmol NH_4F were dissolved in 30 ml water at room temperature to form a yellow solution. The solution was subsequently transferred into a 50 ml Teflon-lined stainless steel autoclave in which as-prepared NF was immersed into the solution, heating at 120 °C for 6 h. After the reaction, the NF was washed by ethanol and deionized water for several times and then dried at 60 °C for overnight in a vacuum drying oven.

2.3. Synthesis of hierarchical CoFe@NiFe/NF core-shell architectures

The NiFe-LDH was grown onto the surface of CoFe-LDH nanosheets by electrodeposition. The reaction was operated in a three-electrode configuration, where the CoFe-LDH was directly used as the working electrode, and a Pt wire and an Ag/AgCl electrode were used as the counter electrode and the reference electrode, respectively. Aqueous solution containing 0.15 M Ni $(NO_3)_2$·6H_2O and 0.15 M FeSO$_4$·7H_2O was used as electrolyte. Typically, the deposition was performed by applying a constant potential of −1.0 V vs Ag/AgCl for 50 s, 100 s, 200 s, 300 s, respectively, and the corresponding samples were denoted as CoFe@NiFe-50/NF, CoFe@NiFe-100/NF, CoFe@NiFe-200/NF, CoFe@NiFe-300/NF, respectively.

2.4. Materials characterization

X-ray diffraction (XRD) data of as-prepared samples were collected from a Bruker D8 Advance X-ray diffractometer with Cu Kα radiation; λ = 1.5406 Å at the range between 10 and 80° 2θ at a scan step of 2°/min. The microstructure of the samples were investigated by using S-4800 II FESEM scanning electron microscopy (SEM) and Tecnai 12 transmission electron microscopy (TEM) at 15 kV and 120 kV, respectively. The high-resolution TEM (HRTEM) was performed on Tecnai G2 F30 S-Twin TEM at an acceleration voltage of 300 kV. X-ray photoelectron spectroscopy (XPS) data were acquired on ECSA PHI500 spectrometer with an Al Kα radiator.

2.5. Electrochemical measurements

Electrodes were tested in a conventional three-electrode system by using a CHI-760D electrochemical workstation (CHI Instruments, Shanghai, China) at room temperature. A 1 cm × 1 cm area of as-prepared NF-based electrocatalysts was used as the working electrode, a platinum mesh as the counter electrode and Ag/AgCl (saturated KCl) electrode as the reference electrode. Prior to the test, the saturated calomel electrode (SCE) calibration was performed by measuring the reversible hydrogen electrode (RHE) potentials with platinum electrodes under the hydrogen, then all potential was converted to the RHE reference scale based on the formula of E_{RHE} = $E_{Ag/AgCl}$ + 0.197 V + 0.059 × pH. Linear sweep voltammetry (LSV) and cyclic voltammetry curves towards HER and OER were measured in 1.0 M KOH (pH = 14.0) at a scan rate of 5 mV s^{-1}. After that, the potentials and voltages calibrate by iR corrected. Electrochemical impedance spectroscopy (EIS) was performed on the same three-electrodes with AC impedance over a frequency range from 0.01 to 10^4 Hz. The electrochemical surface area (ECSA) was obtained by CVs in different scan rates from 0.2 to 1.6 V/s. Overpotential is calculated in this work according to η (V) = E_{RHE} − 1.23.

Electrochemical H_2 and O_2 evolution: Electrochemical H_2 and O_2 evolutions were measured using a CHI-760D electrochemical workstation in a homemade electrochemical device. The CoFe@NiFe-200/
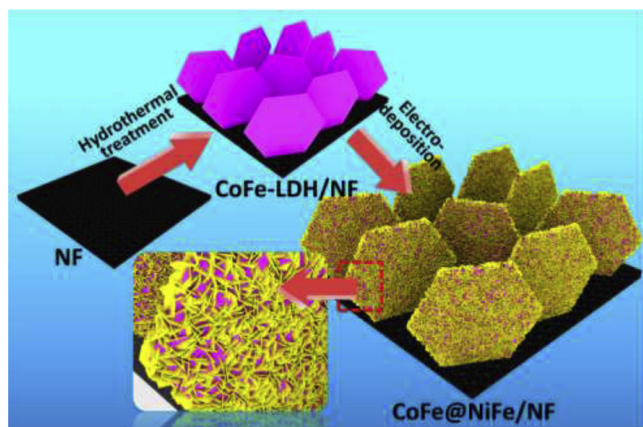
Fig. 1. Schematic diagram for the fabrication of CoFe@NiFe/NF architecture.

NF was used as both the anode and cathode in 1.0 M KOH. The Faraday efficiency (FE%) was calculated by the equation: FE% $= n_g$(experimental)/ n_g(theoretical), where n_g(experimental) is the number of moles of the gas produced and n_g(theoretical) $= Q/zF$, where Q is the charge passed through the electrodes, z means z mole electrons per mole H_2 (z = 2), F is Faraday constant (96,485 $Cmol^{-1}$).

3. Results and discussion

3.1. Characterization of hierarchical CoFe@NiFe/NF core-shell architectures

The synthetic process of hierarchical CoFe@NiFe/NF core-shell architectures is depicted in Fig. 1. Firstly, the CoFe-LDH nanosheet arrays were synthesized on the NF substrate via a facile hydrothermal method. Subsequently, the NiFe-LDH nanosheet was decorated on the CoFe-LDH nanosheet arrays by a fast electrodeposition method, forming hierarchical CoFe@NiFe/NF core-shell architectures. The formation of the CoFe@NiFe/NF can be reflected by the appearance color change of the samples (Figure S1). It is obviously that bare NF became yellow after hydrothermal reaction and then the color changes into deeper after electrodeposition of NiFe-LDH.

The morphologies of the as-prepared samples were firstly illustrated by SEM and TEM. The SEM images (Fig. 2a, b) of CoFe-LDH/NF sample indicates that the CoFe-LDH nanosheets with smooth surface and thicknesses of around 50 nm were erectly growth on the NF substrate, forming 3D interconnected nanosheets arrays, which can act as the ideal conductive scaffolds for the subsequent growth of the NiFe-LDH nanosheets. After electrodeposition, the NiFe-LDH nanosheets were erectly deposited on the CoFe-LDH nanosheet arrays substrate (Fig. 2c, d), forming well-defined hierarchical "nanosheet on nanosheet" architecture. This hierarchical "nanosheet on nanosheet" architecture not only provides enlarged surface area with more active sites for the redox reactions, but also possess open porous structure that can facilitate the fast mass transport and electrolyte penetration, therefore endowing the electrodes with high electrocatalytic performance. It is worth noting that the structure and loading amount of NiFe-LDH nanosheets shell can be modulated by controlling the deposition times (Figure S2). The hierarchical CoFe@NiFe/NF core-shell architectures with the proper NiFe-LDH loading amount possibly possess the maximum interface or optimal electronic interaction contributive to the improvement of electrocatalytic activity. For comparative purpose, the bare NiFe-LDH nanosheet arrays were also deposited on the NF by the similar method as that of CoFe@NiFe-200/NF (Figure S2).

The structure of the hierarchical CoFe@NiFe-200/NF core-shell architecture was further confirmed by the TEM analysis (Fig. 2e). Compared with the smooth surface of CoFe-LDH nanosheet (Figure S3), many tiny nanosheets with thickness of around 6 nm were decorated on

the surface to form hierarchical core-shell architectures with abundant interfaces (Fig. 2f). This architecture with abundant interfaces can provide more exposed active sites, thus promoting the catalytic activity. The lattice fringes of 0.25 nm and 0.263 nm in Fig. 2g correspond to the (012) plane of CoFe-LDH and (012) plane of NiFe-LDH, respectively. The energy-dispersive X-ray spectroscopy (EDS) elemental mapping images (Fig. 2h) demonstrate that the nickel, iron, cobalt and oxygen elements are uniformly distributed throughout the whole CoFe@NiFe-200/NF, indicating that the NiFe-LDH was uniformly aligned the surface of CoFe-LDH nanosheet arrays.

The XRD patterns of as-preaprd CoFe@NiFe core-shell architectures, bare CoFe-LDH/NF, and NiFe-LDH/NF are shown in Fig. 3a and Figure S4. Owing to the strong diffraction intensity of NF substrate compared with the weak peak signals of the electrocatalyst material, the powder are scraped from NF and then measured at the same time. For the bare CoFe-LDH (Fig. 3a), the diffraction peaks at 11.7°, 23.4°, 34.1°, 36.6°, 38.7°, 43.3°, 46.2°, 52.4°, 56.0°, 59.1°, 60.5° and 63.4° can be assigned to (003), (006), (012), (104), (015), (107), (018), (10 10), (01 11), (110), (113) and (10 13) planes (JCPDS Card no. 50-0235), respectively [47,48]. For the bare NiFe-LDH, the diffraction peaks at 22.9°, 33.5°, 34.4°, 38.9°, 59.9°, 61.2°, 65.1° and 71.2° can be correspond to the (006), (101), (012), (015), (110), (113), (116) and (119) planes of NiFe-LDH (JCPDS Card no. 40-0215) [49]. In the CoFe@NiFe-200/NF sample, all the diffraction peaks can be assigned either to the CoFe-LDH or to the NiFe-LDH, and no other impurity phase can be found, indicating the formation of hierarchical CoFe@NiFe-200/NF core-shell architecture.

To further investigate the surface chemical state and electronic structure of CoFe@NiFe-200/NF, XPS was performed. In Fig. 3b, the high resolution spectra of Co 2p for CoFe-LDH shows the binding energies of Co $2p_{3/2}$ and Co $2p_{1/2}$ at 780.8 eV and 796.7 eV, respectively, implying the presence of a high-spin Co^{2+} state [50,51]. The peaks at 785.7 and 802.9 eV can be ascribed to the satellite peaks. Comparably, the peaks of Co $2p_{3/2}$ and Co $2p_{1/2}$ of CoFe@NiFe-200/NF have a slightly negative shift by 0.07 and 0.13 eV towards higher binding, respectively, indicating that there is a strong interfacial interaction between CoFe-LDH and NiFe-LDH [52]. The Fe 2p core-level spectra (Fig. 3c) of CoFe-LDH have two spin orbit peaks located at 724.3 and 710.5 eV, which could be ascribed to the Fe $2p_{3/2}$ and Fe $2p_{1/2}$ of Fe^{3+} [53]. It is obvious that, compared to CoFe-LDH, the binding energies of Fe $2p_{3/2}$ and Fe $2p_{1/2}$ of the CoFe@NiFe-200/NF sample show a negative shift of 1.1 and 0.3 eV. These negative shifts suggest the presence of strong interfacial electronic interactions of between CoFe-LDH and NiFe-LDH, which is vital for the fast charge transfer in the HER process. In Fig. 3d, the two major peaks of NiFe-LDH located at binding energies of 856.2 and 873.8 eV corresponds to Ni $2p_{3/2}$ and Ni $2p_{1/2}$, respectively, along with two shakeup satellites at 862.0 and 880.0 eV relate to Ni^{2+} and Ni^{3+} [54]. In contrast, the peaks of both the Ni $2p_{3/2}$ and Ni $2p_{1/2}$ have an obvious shift, indicating the existence of strong electronic interactions between the CoFe-LDH and NiFe-LDH in the CoFe@NiFe-200/NF core-shell architecture.

3.2. Oxygen evolution reaction performance

In order to evaluate the OER activity, the hierarchical CoFe@NiFe/NF core-shell architectures was measured by using a standard three-electrode system in O_2-saturated 1.0 M KOH. To reach a steady state, all catalysts were prepared by electrochemically pre-conditioned. Fig. 4a shows the polarization curves of the different electrocatalysts after *iR*-drop corrections. The non-characteristic polarization curves of the bare NF ensure the minimum background. The CoFe@NiFe-200/NF core-shell architecture displays the remarkable catalytic with low η_{10} of only 190 mV. It obviously outperforms the samples of CoFe-LDH/NF (240 mV), NiFe-LDH/NF (270 mV), CoFe@NiFe-50/NF (230 mV), CoFe@NiFe-100/NF (220 mV), and CoFe@NiFe-300/NF (223 mV) (Fig. 4c). Notably, as compared with recently reported electrocatalysts,
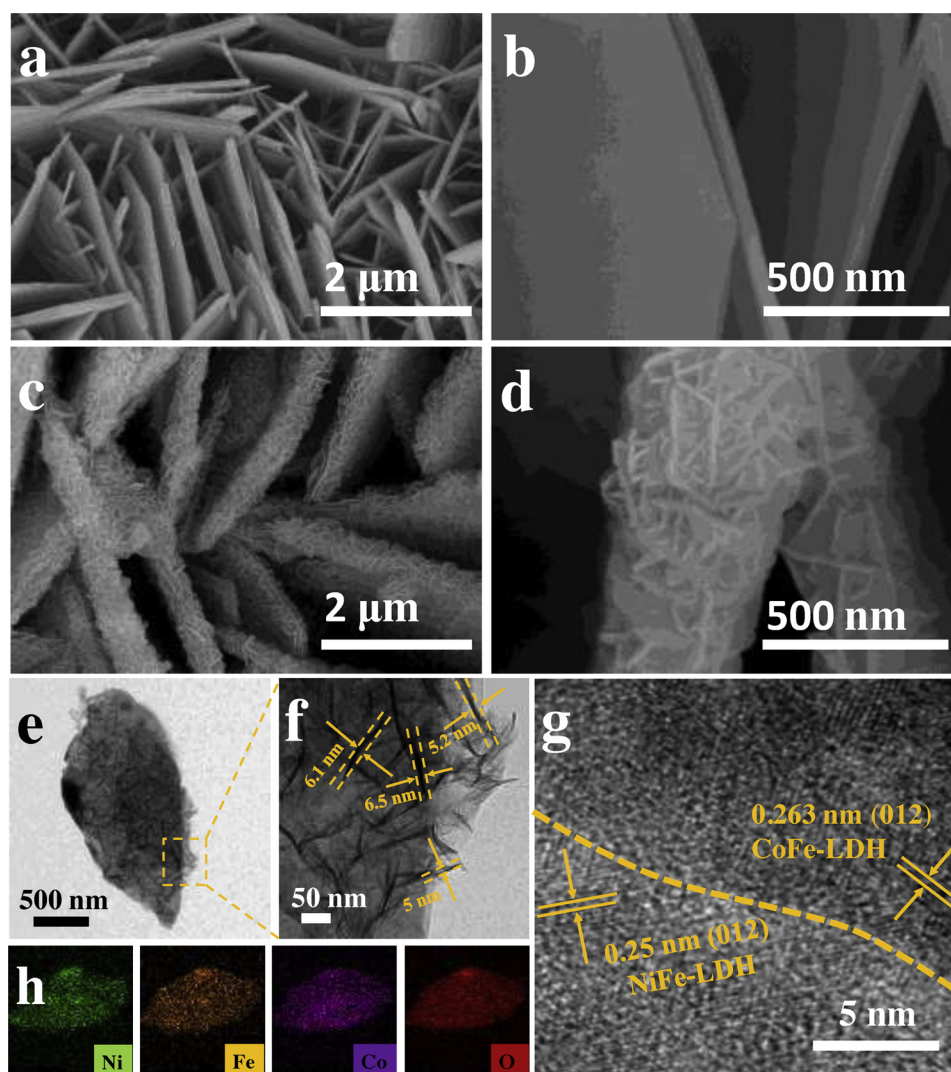
Fig. 2. SEM images of (a, b) CoFe-LDH/NF and (c, d) CoFe@NiFe-200/NF architecture. (e) TEM, (f) magnified TEM image, (g) HRTEM image, and (h) elemental mapping images of CoFe@NiFe-200/NF architecture.

the as-prepared CoFe@NiFe-200/NF performs outstandingly among them, such as CoNiP@LDH (230 mV) [44], CoFe-LDH@CoFe-Bi (418 mV) [55], Ni$_{0.8}$Fe$_{0.2}$ (206 mV) [14], and Fe$_1$Co$_1$-ONS (308 mV) [56] and other catalysts (Table S4).

In quest of the OER reaction kinetics, Tafel plots derived from the LSV curves in Fig. 4a (from 1.2 to 1.6 V), and the Tafel slope were calculated by the Tafel equation: $\eta = b \log j + a$ (where η represents overpotential, b refers to Tafel slope, and j is on behalf of the current density). The Tafel slope of CoFe@NiFe-200/NF core-shell architecture is evaluated to be 45.71 mV dec^{-1}, which is much smaller than CoFe-LDH/NF (65.07 mV dec^{-1}), NiFe-LDH/NF (67.44 mV dec^{-1}) and other catalysts with different deposition times (Fig. 5a and Figure S5), i.e., CoFe@NiFe-50/NF (63.3 mV dec^{-1}), CoFe@NiFe-300/NF (60.62 mV dec^{-1}), and CoFe@NiFe-300/NF (49.12 mV dec^{-1}). Remarkably, the slope value significantly magnifies favorable OER kinetics in the CoFe@NiFe-200/NF.

To understand the electron transport capacity, the electrochemical impedance spectroscopy (EIS) was measured in 1.0 M KOH. The semicircles of the Nyquist plot on behalf of the charge transfer resistance (R$_{ct}$), and the smaller semicircles suggest the rapid charge transfer at the interface. The outstanding OER performance of CoFe@NiFe-200/NF core-shell architecture stemmed from fast charge transfer which can also be observed in the smallest semicircles among as-prepared catalysts. As shown in Fig. 5b, CoFe@NiFe-200/NF exhibits much smaller

R$_{ct}$ (0.92 Ω) than CoFe-LDH/NF (2.8 Ω), NiFe-LDH/NF (2.22 Ω), CoFe@NiFe-50/NF (1.18 Ω), CoFe@NiFe-100/NF (0.98 Ω), CoFe@NiFe-300/NF (1.08 Ω) (Table S1), indicating that CoFe@NiFe-200/NF owned faster electron transport kinetics at the interface between electrodes and electrolyte.

It is significant for catalysts to possess large electrochemical active surface areas (ECSA) which can provide more exposed active sites for the electrocatalytic reaction. The ECSA was estimated using the formula: ECSA = C$_{dl}$/C$_s$, where C$_{dl}$ is the electrochemical double-layer capacitance, and C$_s$ is the specific capacitance of a flat surface of the electrode material among 20–60 μF cm$_{ECSA}^{-2}$ [30,57]. The C$_{dl}$ was measured via cyclic voltammograms in the region of 1.022–1.112 V vs RHE at the scan rates ranging from 20 to 160 mV s^{-1} without Faradaic currents (Figure S6). As shown in Fig. 5c, CoFe@NiFe-200/NF possesses highest C$_{dl}$ among all the samples, which is almost 3 times larger than CoFe-LDH/NF, NiFe-LDH/NF, CoFe@NiFe-50/NF, CoFe@NiFe-100/NF, and CoFe@NiFe-300/NF. Apparently, this high C$_{dl}$ value indicates that the hierarchical CoFe@NiFe core-shell architectures expose a great number of more active sites, contributing to the enhanced OER activity. Nevertheless, such a small variation in C$_{dl}$ is unlikely to fully explain the large differences in catalytic performance. Hence, we then normalized the current density to C$_{dl}$, and it is found that CoFe@NiFe-200/NF core-shell architectures exhibit greater specific current density (Figure S7), indicating that CoFe@NiFe-200/NF is intrinsically more
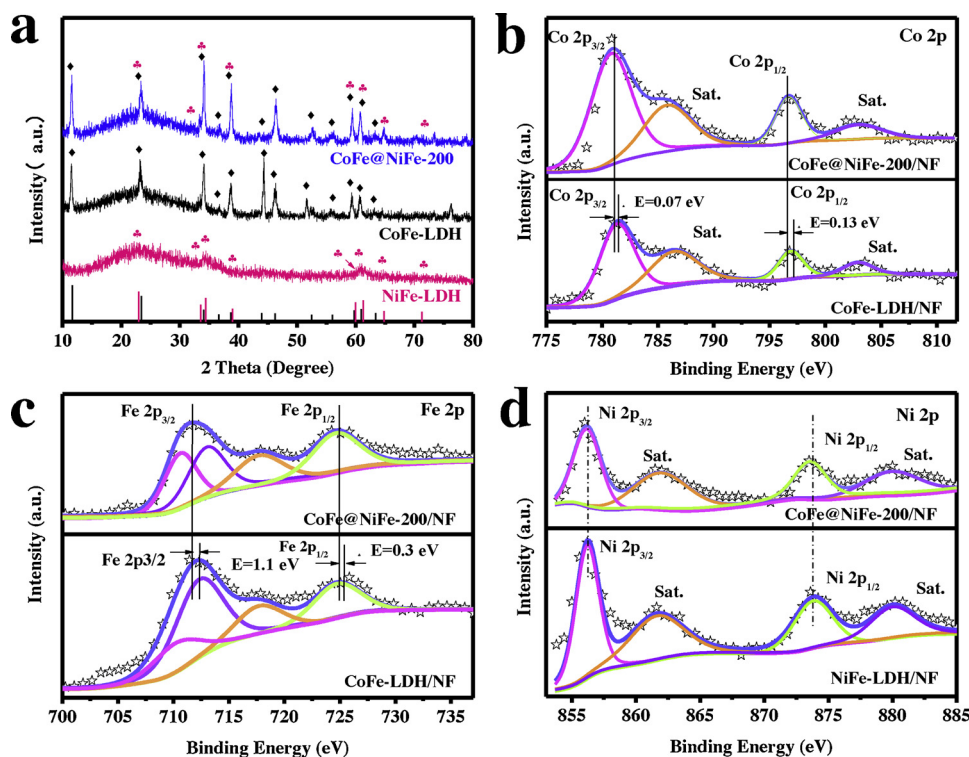
Fig. 3. (a) XRD patterns of CoFe-LDH, NiFe-LDH and CoFe@NiFe-200; (b–d) XPS spectra of CoFe-LDH/NF and CoFe@NiFe-200/NF of (b) Co 2p, (c) Fe 2p, (d) Ni 2p narrow-scan spectra.

active than other CoFe@NiFe/NF composites.

The turnover frequency (TOF) is a commonly used parameter to evaluate the intrinsic catalytic activity of each catalytic site. The TOF value can be calculated by the equation: TOF = $(jA)/(4Fn)$, where j is the current density at a constant overpotential, A is the area of the working electrode, F is Faraday's constant (96,485.3 C mol^{-1}) and n is

the number of moles of the active materials. Indeed, we assumed that all active surface sites were acted in the reaction. The calculated TOF of CoFe@NiFe-200/NF architecture is 11.9 s^{-1}, which is about 16.5-, 13.5-, 5.9-, 4.9- and 1.45-fold than that of bare CoFe-LDH/NF, NiFe-LDH/NF, CoFe@NiFe-50/NF, CoFe@NiFe-100/NF, and CoFe@NiFe-300/NF at the overpotential of 300 mV, respectively (Table S2). This
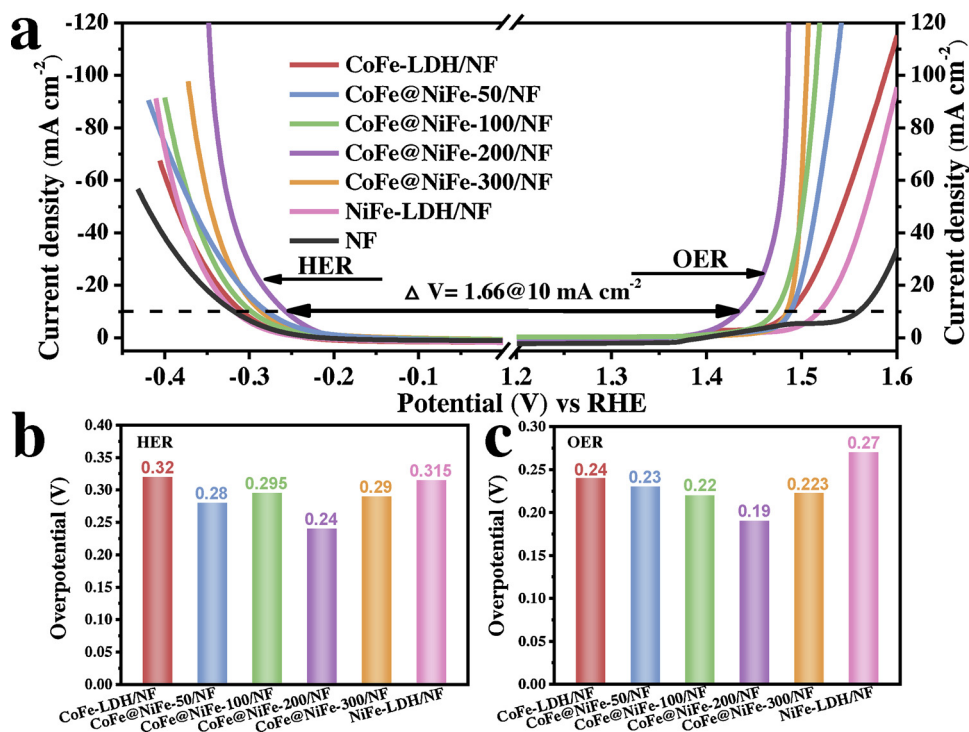
Fig. 4. (a) Steady-state polarization curves of CoFe-LDH/NF, CoFe@NiFe-50/NF, CoFe@NiFe-100/NF, CoFe@NiFe-200/NF, NiFe-300/NF, NiFe-LDH/NF and NF in 1.0 M KOH for HER and OER; (b) overpotential at current density of 10 mA cm^{-2} for HER; (c) overpotential at current density of 10 mA cm^{-2} for OER.
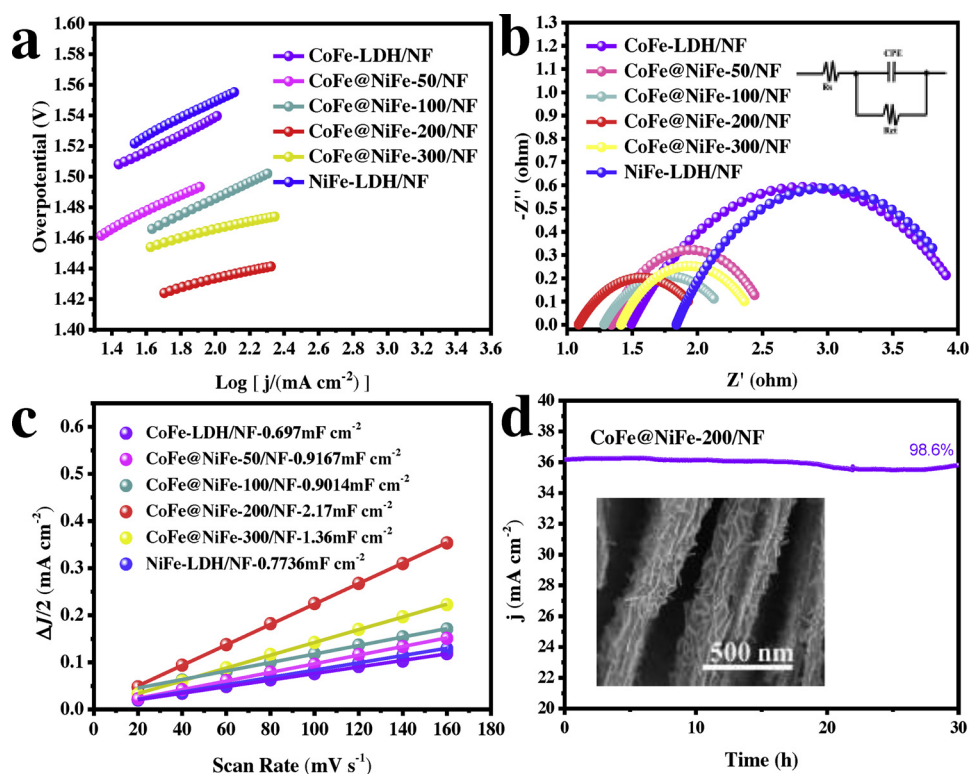
Fig. 5. OER performance of CoFe-LDH/NF, NiFe-LDH/NF and a series of CoFe@NiFe/NF catalysts: (a) corresponding Tafel plots derived from steady-state polarization curves in 1.0 M KOH for OER; (b) Nyquist plots of CoFe@NiFe/NF samples with the fitting curves; (c) capacitive $(\Delta J/2 = (J_a - J_c)/2)$ vs scan rate of as-made samples and the corresponding linear slopes; (d) chronoamperometric curves (I-t) of CoFe@NiFe-200/NF at the constant overpotential of 320 mV.

striking increase of TOF highlights its excellent performance of CoFe@NiFe-200/NF core-shell architecture for OER catalysis.

Long-term stability is a key parameter for an electrocatalyst that determines whether it can be widely used in industry. As shown in Fig. 5d, the I-t curve shows that CoFe@NiFe-200/NF exhibit the outstanding stable OER behavior with a constant overpotential after 30 h in alkaline solution and the CoFe@NiFe-200/NF electrode also keep the original morphology without apparent shedding (Fig. 5d, inset). Moreover, the polarization curve of CoFe@NiFe-200/NF approximates to the initial one after 1000 CVs (Figure S8), indicating that CoFe@NiFe-200/NF possesses superior stability and durability in alkaline solution.

3.3. Hydrogen evolution reaction performance

The HER activity of samples was also investigated in a three-electrode system in Ar-saturated 1.0 M KOH. All potentials were referenced to the reversible hydrogen electrode (RHE), with iR compensation. As shown in Fig. 4a (from −0.45 V to 0 V), CoFe@NiFe-200/NF shows the highest HER activities with a low overpotential (η_{10}) of 240 mV, which is much lower than those of CoFe-LDH/NF (320 mV), CoFe@NiFe-50/NF (280 mV), CoFe@NiFe-100/NF (295 mV), CoFe@NiFe-300/NF (290 mV), and NiFe-LDH/NF (315 mV). Moreover, the HER activity of the different electrocatalyst was also evaluated by Tafel plots. As shown in Fig. 6a and Figure S9, the CoFe@NiFe-200/NF exhibited a small Tafel slope of 88.88 mV dec^{-1}, much smaller than CoFe-LDH/NF (127.33 mV dec^{-1}), CoFe@NiFe-50/NF (100.84 mV dec^{-1}), CoFe@NiFe-100/NF (104.51 mV dec^{-1}), CoFe@NiFe-300/NF (97.73 mV dec^{-1}) and NiFe-LDH/NF (108 mV dec^{-1}). This low Tafel slop value of CoFe@NiFe-200/NF indicates the outstanding kinetics of HER reaction, which is attributed to the synergistic effect of the CoFe-LDH and NiFe-LDH. Notably, the HER activity of the current CoFe@NiFe-200/NF is comparable with or even superior to many state-of-the-art HER electrocatalysts (Table S5).

To explore the insight of electron transportation capability, EIS was measured in Ar-saturated 1 M KOH aqueous solution. As shown in

Nyquist plots of the EIS spectra in Fig. 6b and Table S3, the charge transfer resistance decrease from CoFe-LDH/NF ($R_{ct} = 11.2 \ \Omega$) to CoFe@NiFe-200/NF ($R_{ct} = 3.74 \ \Omega$), suggesting that charge transport efficiency of CoFe@NiFe-200/NF can facilitate the combination between electrons and H_{ads}, and enable effective electrical integration to minimize parasitic Ohmic losses. Then, the ECSA was estimated based on the C_{dl} obtained via cyclic voltammetry (Figure S10) and the results are shown in Fig. 6c. The CoFe@NiFe core-shell architectures possess the largest C_{dl}, which is near 2.5 times larger than that of CoFe-LDH, indicating that the formation of hierarchical CoFe@NiFe core-shell architecture can enlarge the active specific area and provide more accessible active sites for the HER reaction. In addition, the synergistic effect of CoFe-LDH core and NiFe-LDH shell could possibly facilitate the adsorption and dissociation of H_2O. Thus the HER performance could be effectively improved. The calculated TOF value of CoFe@NiFe-200/NF core-shell architecture is 15.7 s^{-1}, which is far exceed the samples of CoFe-LDH/NF (0.968 s^{-1}), NiFe-LDH/NF (0.962 s^{-1}), CoFe@NiFe-50/NF (3.36 s^{-1}), CoFe@NiFe-100/NF (3.82 s^{-1}) and CoFe@NiFe-300/NF (9.36 s^{-1}) at the overpotential of 220 mV, respectively (Table S2).

The cycling stability of the CoFe@NiFe-200/NF for the HER performance was investigated. The I-t curve in Fig. 6d exhibit that CoFe@NiFe-200/NF possess the excellent stability for maintaining the original current density within continue 30 h at a current density of 10 mA cm^{-2} in alkaline solution. In addition, the polarization curves for CoFe@NiFe-200/NF after 1000 CVs measured at a scan rate of 50 mV s^{-1} only increase 1 mV than the initial one (Figure S11). Furthermore, the original morphology of the CoFe@NiFe-200/NF after the stability test was still retained, exhibiting the outstanding stability of CoFe@NiFe-200/NF (Fig. 6d, inset).

3.4. Overall water splitting performance

Owing to the CoFe@NiFe-200/NF exhibits outstanding bifunctional OER and HER properties, we fabricate a two-electrode system to assess its performance for overall water splitting by using CoFe@NiFe-200/NF
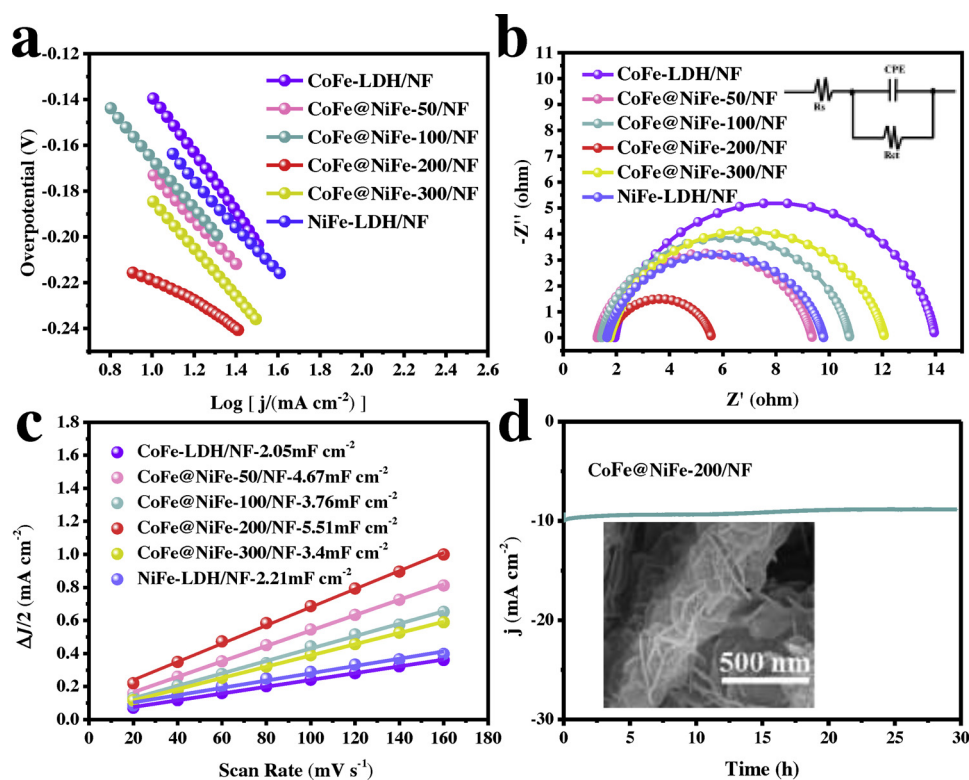
Fig. 6. HER performance of CoFe-LDH/NF, NiFe-LDH/NF and a series of CoFe@NiFe/NF catalysts: (a) corresponding Tafel plots derived from steady-state polarization curves in 1.0 M KOH for OER; (b) Nyquist plots of CoFe@NiFe/NF samples with the fitting curves; (c) capacitive $(\Delta J/2 = (J_a - J_c)/2)$ vs scan rate of as-made samples and the corresponding linear slopes; (d) chronoamperometric curves (I-t) of CoFe@NiFe-200/NF.
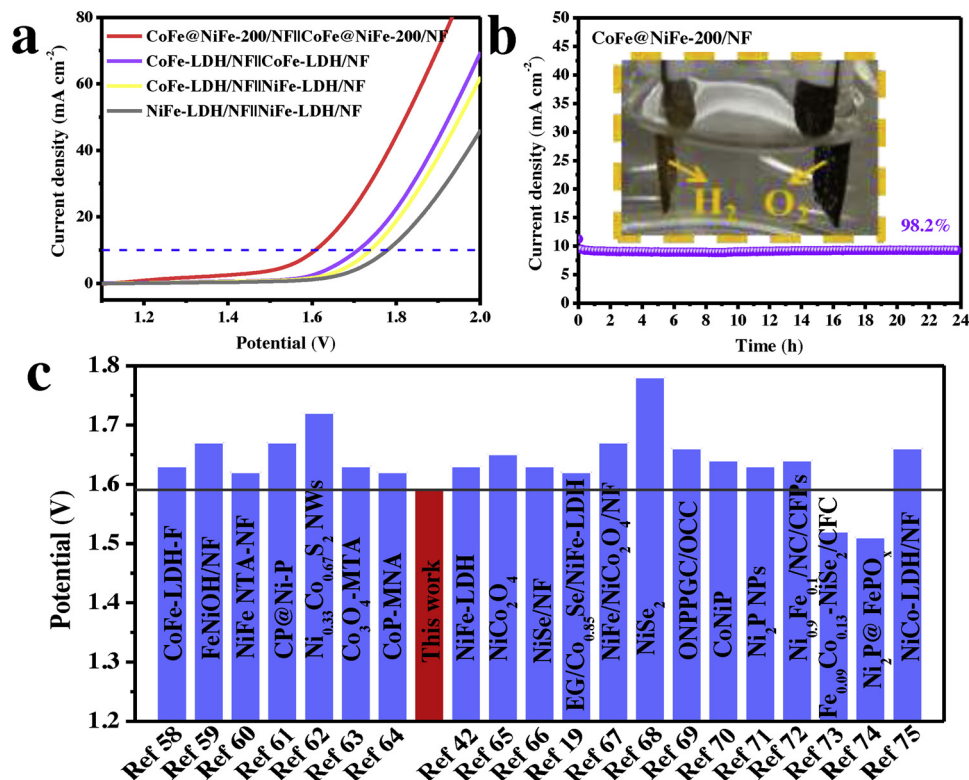

Fig. 7. (a) LSV results of two-electrode cell assembled by various materials; (b) durability test of electrolyzer constructed by CoFe@NiFe-200/NF at 10 mA cm^{-2} for 24 h, inset shows the photo of the electrolyzer; (c) comparison of potentials at 10 mA cm^{-2} of this work with the reported bifunctional electrocatalysts in two-electrode water-splitting systems.

for both anode and cathode. As shown in Fig. 7a, the electrolytic process achieved a potential of 1.59 V at the current density of 10 mA cm^{-2}, significantly superior to the CoFe-LDH/NF||CoFe-LDH/NF (1.7 V), CoFe-LDH/NF||CoFe@NiFe-200/NF (1.73 V), NiFe-LDH/NF||NiFe-LDH/NF (1.78 V) in 1.0 M KOH. In addition, the electrolytic potential hold steady within 24 h, indicating that is excellent long-term stability in overall water splitting (Fig. 7b). From the inset in Fig. 7b, it

can be observed that abundant hydrogen and oxygen gas bubbles were generated from the cathode and the anode, respectively, suggesting the excellent water splitting performance. It is worth noting that the current CoFe@NiFe-200/NF||CoFe@NiFe-200/NF outperforms many other reported electrolyzers for overall water splitting (Fig. 7c) [19,42,58–75], such as EG/Co$_{0.85}$Se/NiFe-LDH (1.67 V) [19], NiFe-LDH (1.63 V) [42], CoFe-LDH-F (1.63 V) [58], comparable to the some high-

performance electrolyzers such as $Fe_{0.09}Co_{0.13}$-$NiSe_2$/CFC (1.52 V) [73] and $Ni_2P@FePO_x$ (1.51 V) [74]. To explore the utilization efficiency of electrons participate in an electrochemical system, we measured the Faradaic efficiency (FE) in 1.0 M KOH. As shown in Figure S12, the gas volume of H_2 and O_2 are in good agreement of the theoretical value, and the FE is calculated to be approximately 99.3%. The H_2 or O_2 production rates are approximately 0.30 mmol h^{-1} and 0.15 mmol h^{-1}, respectively, with the atomic ratio of H_2 and O_2 being close to 2:1, suggesting that water is completely decomposed into oxygen and hydrogen.

The excellent bifunctional OER and HER performances and stabilities of the as-prepared CoFe@NiFe-200/NF core-shell architectures can be ascribed to the following factors: (i) the strong electronic interaction between CoFe-LDH and NiFe-LDH not only facilitates the fast charge transfer at the interface, but also synergistically optimize the binding energies of the reaction intermediates, thus accelerating the reaction kinetics and enhancing the electrocatalytic efficiency. (ii) The formed CoFe@NiFe/NF core-shell architectures with 3D interconnected porous structure provide abundant accessible active sites and contact with electrolytes closely, which is beneficial for the ion diffusion and gas release. (iii) The direct growth on Ni foam not only guarantees the good electric conductivity thus favors fast electron transport, but also enables the good mechanical adhesion, therefore leading to an excellent electrocatalytic activities and stabilities.

4. Conclusions

In summary, we have developed a novel hierarchical CoFe@NiFe-200/NF core-shell architecture for water splitting in alkaline solution. The as-prepared CoFe@NiFe-200/NF electrocatalyst exhibits excellent bifunctional activities and stabilities for OER and HER. We attributed this high activity to the strong synergistic effect of the CoFe-LDH and NiFe-LDH and the typical 3D interconnected architectures, which can contribute to the fast charge transfer and mass transport, optimize the binding energies of the reaction intermediates, thus enhancing the catalytic performance. Furthermore, we have achieved a voltage of 1.59 V at the current density of 10 mA cm^{-2} by using the CoFe@NiFe-200/NF as both the cathode and anode, which is superior to many other reported electrolyzers for overall water splitting. Given the high electrocatalytic activity and stability, together with its low cost and natural abundance of LDH materials, it is expected that the present CoFe@NiFe/NF electrocatalyst hold great promising in the practical alkaline overall water splitting.

Acknowledgements

Appendix A. Supplementary data

Supplementary material related to this article can be found, in the online version, at doi:https://doi.org/10.1016/j.apcatb.2019.04.054.

References

[1] Y.R. Zheng, P. Wu, M.R. Gao, X.L. Zhang, F.Y. Gao, H.X. Ju, R. Wu, Q. Gao, R. You, W.X. Huang, S.J. Liu, S.W. Hu, J.F. Zhu, Z.Y. Li, S.H. Yu, Doping-induced structural phase transition in cobalt diselenide enables enhanced hydrogen evolution catalysis, Nat. Commun. 9 (2018) 2533.

[2] Y.P. Liu, G.T. Yu, G.D. Li, G.D. Li, Y.H. Sun, T. Asefa, W. Chen, X.X. Zou, Coupling Mo_2C with nitrogen-rich nanocarbon leads to efficient hydrogen-evolution electrocatalytic sites, Angew. Chem. Int. Edit. 54 (2015) 10752–10757.

[3] M. Zhou, Q. Weng, Z.I. Popov, Y. Yang, L.Y. Antipina, P.B. Sorokin, X. Wang, Y. Bando, D. Golberg, Construction of polarized carbon–nickel catalytic surfaces for potent, durable, and economic hydrogen evolution reactions, ACS Nano 12 (2018)

[4] L. Liu, D. Li, H.P. Zhao, A. Dimitrova, L.H. Li, Y.G. Fang, J. Krischok, W.D. Shi, Y. Lei, Optimizing hydrogen evolution activity of nanoporous electrodes by dual-step surface engineering, Appl. Catal. B-Environ. 244 (2019) 87–95.

[5] X.M. Xu, Y.B. Chen, W. Zhou, Z.H. Zhu, C. Su, M.L. Liu, Z.P. Shao, A perovskite electrocatalyst for efficient hydrogen evolution reaction, Adv. Mater. 28 (2016) 6442–6448.

[6] Y. Wu, F. Li, W.L. Chen, Q. Xiang, Y.L. Ma, H. Zhu, P. Tao, C.Y. Song, W. Shang, T. Deng, J.B. Wu, Coupling interface constructions of $MoS_2/Fe_5Ni_4S_8$ heterostructures for efficient electrochemical water splitting, Adv. Mater. 30 (2018) 1803151.

[7] T.R. Zhan, X.L. Liu, S.S. Lu, W.G. Hou, Nitrogen doped NiFe layered double hydroxide/reduced graphene oxide mesoporous nanosphere as an effective bifunctional electrocatalyst for oxygen reduction and evolution reactions, Appl. Catal. B-Environ. 205 (2017) 551–558.

[8] T. Kosmala, H.C. Diaz, H.P. Komsa, Y. Ma, A.V. Krasheninnikov, M. Batzill, S. Agnoli, Metallic twin boundaries boost the hydrogen evolution reaction on the basal plane of molybdenum selenotellurides, Adv. Energy Mater. 8 (2018) 1800031.

[9] X.M. Xu, W. Wang, W. Zhou, Z.P. Shao, Recent advances in novel nanostructuring methods of perovskite electrocatalysts for energy-related applications, Small Methods 2 (2018) 1800071.

[10] X.M. Xu, Y.B. Chen, W. Zhou, Y.J. Zhong, D.Q. Guan, Z.P. Shao, Earth-abundant Silicon for facilitating water oxidation over iron-based perovskite electrocatalysts, Adv. Mater. Interfaces 5 (2018) 1701693.

[11] B. Šljukić, M. Vujković, L. Amaral, D.M.F. Santos, R.P. Rocha, C.A.C. Sequeira, J.L. Figueiredo, Carbon-supported Mo_2C electrocatalysts for hydrogen evolution reaction, J. Mater. Chem. A 3 (2015) 15505–15512.

[12] C. Ray, S.C. Lee, K.V. Sankar, B.J. Jin, J. Lee, J.H. Park, S.C. Jun, Amorphous phosphorus-incorporated cobalt molybdenum sulfide on carbon cloth: an efficient and stable electrocatalyst for enhanced overall water splitting over entire pH values, ACS Appl. Mater. Interfaces 9 (2017) 37739–37749.

[13] L. Jiao, Y.X. Zhou, H.L. Jiang, Metal-organic framework-based CoP/reduced graphene oxide: high-performance bifunctional electrocatalyst for overall water splitting, Chem. Sci. 7 (2016) 1690–1695.

[14] M.Q. Yao, N. Wang, W.C. Hu, S. Komarneni, Novel hydrothermal electrodeposition to fabricate mesoporous film of $Ni_{0.8}Fe_{0.2}$ nanosheets for high performance oxygen evolution reaction, Appl. Catal. B-Environ. 233 (2018) 226–233.

[15] X. Wang, F. Li, W.Z. Li, W.B. Gao, Y. Tang, R. Li, Hollow bimetallic cobalt-based selenide polyhedrons derived from metal–organic framework: an efficient bifunctional electrocatalyst for overall water splitting, J. Mater. Chem. A 5 (2017) 17982–17989.

[16] X.M. Xu, C. Su, W. Zhou, Y.L. Zhu, Y.B. Chen, Z.P. Shao, Co-doping strategy for developing perovskite oxides as highly efficient electrocatalysts for oxygen evolution reaction, Adv. Sci. 3 (2016) 1500187.

[17] Y.C. Pi, Q. Shao, P.T. Wang, F. Lv, S.J. Guo, J. Guo, X.Q. Huang, Trimetallic oxyhydroxide coralloids for efficient oxygen evolution electrocatalysis, Angew. Chem. 129 (2017) 4573–4577.

[18] X.J. Liu, W. Xi, C. Li, X.B. Li, J. Shi, Y.L. Shen, J. He, L.H. Zhang, L. Xie, X.M. Sun, P. Wang, J. Luo, L.M. Liu, Y. Ding, Nanoporous Zn-doped Co_3O_4 sheets with single-unit-cell-wide lateral surfaces for efficient oxygen evolution and water splitting, Nano Energy 44 (2018) 371–377.

[19] A.P. Wu, Y. Xie, H. Ma, C.G. Tian, Y. Gu, H.J. Yan, X.M. Zhang, G.Y. Yang, H.G. Fu, Integrating the active OER and HER components as the heterostructures for the efficient overall water splitting, Nano Energy 44 (2018) 353–363.

[20] J.H. Song, C.Z. Zhu, B.Z. Xu, S.F. Fu, M.H. Engelhard, R.F. Ye, D. Du, S.P. Beckman, Y.H. Lin, Bimetallic cobalt-based phosphide zeolitic imidazolate framework: CoP_x phase-dependent electrical conductivity and hydrogen atom adsorption energy for efficient overall water splitting, Adv. Energy Mater. 7 (2017) 1601555.

[21] Y.X. Liu, Y. Bai, Y. Han, Z. Yu, S.M. Zhang, G.H. Wang, J.H. Wei, Q.B. Wu, K.N. Sun, Self-supported hierarchical FeCoNi-LTH/$NiCo_2O_4$/CC electrodes with enhanced bifunctional performance for efficient overall water splitting, ACS Appl. Mater. Interfaces 9 (2017) 36917–36926.

[22] N. Xu, G.X. Cao, Z.J. Chen, Q. Kang, H.B. Dai, P. Wang, Cobalt nickel boride as an active electrocatalyst for water splitting, J. Mater. Chem. A 5 (2017) 12379–12384.

[23] Y. Hou, M.R. Lohe, J. Zhang, S.H. Liu, X.D. Zhuang, X.L. Feng, Vertically oriented cobalt selenide/NiFe layered-double-hydroxide nanosheets supported on exfoliated graphene foil: an efficient 3D electrode for overall water splitting, Energy Environ. Sci. 9 (2016) 478–483.

[24] Y. Zhang, Y.L. Ma, Y.Y. Chen, L. Zhao, L.B. Huang, H. Luo, W.J. Jiang, X. Zhang, S. Niu, D.J. Gao, J. Bi, G.Y. Fan, J.S. Hu, Encased copper boosts the electrocatalytic activity of N-doped carbon nanotubes for hydrogen evolution, ACS Appl. Mater. Interfaces 9 (2017) 36857–36864.

[25] C. Wu, J.H. Li, Unique Hierarchical Mo_2C/C nanosheet hybrids as active electrocatalyst for hydrogen evolution reaction, ACS Appl. Mater. Interfaces 9 (2017) 41314–41322.

[26] A. Kumar, S. Bhattacharyya, Porous NiFe-oxide nanocubes as bifunctional electrocatalysts for efficient water-splitting, ACS Appl. Mater. Interfaces 9 (2017) 41906–41915.

[27] C. Lu, J.Y. Wang, S. Czioska, H. Dong, Z.F. Chen, Hierarchically structured Cu-based electrocatalysts with nanowires array for water splitting, J. Phys. Chem. C 121 (2017) 25875–25881.

[28] P. Zhou, Y.Y. Wang, C. Xie, C. Chen, H.W. Liu, R. Chen, J. Huo, S.Y. Wang, Acid-etched layered double hydroxides with rich defects for enhancing the oxygen evolution reaction, Chem. Commun. 53 (2017) 11778–11781.

[29] J.H. Wang, W. Cui, Q. Liu, Z.C. Xing, A.M. Asiri, X.P. Sun, Recent progress in cobalt-based heterogeneous catalysts for electrochemical water splitting, Adv. Mater. 28

(2016) 215–230.

[30] Y.Q. Yang, W.B. Zhang, Y.L. Xiao, Z.P. Shi, X.M. Cao, Y. Tang, Q.S. Gao, CoNiSe₂ heteronanorods decorated with layered-double-hydroxides for efficient hydrogen evolution, Appl. Catal. B-Environ. 242 (2019) 132–139.

[31] X.T. Han, C. Yu, J. Yang, C.T. Zhao, H.W. Huang, Z.B. Liu, P.M. Ajayan, J.S. Qiu, Mass and charge transfer coenhanced oxygen evolution behaviors in CoFe-layered double hydroxide assembled on graphene, Adv. Mater. Interfaces 3 (2016) 1500782.

[32] M.Z. Yu, S. Zhou, Z.Y. Wang, J.J. Zhao, J.S. Qiu, Boosting electrocatalytic oxygen evolution by synergistically coupling layered double hydroxide with MXene, Nano Energy 44 (2018) 181–190.

[33] J. Hu, C.X. Zhang, L. Jiang, H. Lin, Y.M. An, D. Zhou, M.K.H. Leung, S.H. Yang, Nanohybridization of MoS₂ with layered double hydroxides efficiently synergizes the hydrogen evolution in alkaline media, Joule 1 (2017) 383–393.

[34] H.J. Zhang, X.P. Li, A. Hähnel, V. Naumann, C. Lin, S. Azimi, S.L. Schweizer, A.W. Maijenburg, R.B. Wehrspohn, Bifunctional heterostructure assembly of NiFe LDH nanosheets on NiCoP nanowires for highly efficient and stable overall water splitting, Adv. Funct. Mater. 28 (2018) 1706847.

[35] Y.Y. Wang, D.F. Yan, S.E. Hankari, Y.Q. Zou, S.Y. Wang, Recent progress on layered double hydroxides and their derivatives for electrocatalytic water splitting, Adv. Sci. 5 (2018) 1800064.

[36] Z.J. Wang, D.W. Cao, L.Y. Wen, R. Xu, M. Obergfell, Y. Mi, Z.B. Zhan, N. Nasori, J. Demsar, Y. Lei, Manipulation of charge transfer and transport in plasmonic-fer-roelectric hybrids for photoelectrochemical applications, Nat. Commun. 7 (2016) 10348.

[37] L. Yu, H.Q. Zhou, J.Y. Sun, F. Qin, D. Luo, L.X. Xie, F. Yu, J.M. Bao, Y. Li, Y. Yu, S. Chen, Z.F. Ren, Hierarchical Cu@CoFe layered double hydroxide core-shell na-noarchitectures as bifunctional electrocatalysts for efficient overall water splitting, Nano Energy 41 (2017) 327–336.

[38] Y. Jia, L.Z. Zhang, G.P. Gao, H. Chen, B. Wang, J.Z. Zhou, M.T. Soo, M. Hong, X.C. Yan, G.R. Qian, J. Zou, A.J. Du, X.D. Yao, A heterostructure coupling of ex-foliated Ni-Fe hydroxide nanosheet and defective graphene as a bifunctional elec-trocatalyst for overall water splitting, Adv. Mater. 29 (2017) 1700017.

[39] L. Yu, H.Q. Zhou, J.Y. Sun, F. Qin, F. Yu, J.M. Bao, Y. Yu, S. Chen, Z.F. Ren, Cu nanowires shelled with NiFe layered double hydroxide nanosheets as bifunctional electrocatalysts for overall water splitting, Energy Environ. Sci. 10 (2017) 1820–1827.

[40] L.B. Gao, H.T. Zhang, J.U. Surjadi, P.F. Li, Y. Han, D. Sun, Y. Lu, Mechanically stable ternary heterogeneous electrodes for energy storage and conversion, Nanoscale 10 (2018) 2613–2622.

[41] G.B. Chen, T. Wang, Zhang J, P. Liu, H.J. Sun, X.D. Zhuang, M.W. Chen, X.L. Feng, Accelerated hydrogen evolution kinetics on NiFe-layered double hydroxide elec-trocatalysts by tailoring water dissociation active sites, Adv. Mater. 30 (2018) 1706279.

[42] J.S. Luo, J.H. Im, M.T. Mayer, M. Schreier, M.K. Nazeeruddin, N.G. Park, S.D. Tilley, H.J. Fan, M. Grätzel, Water photolysis at 12.3% efficiency via perovskite photovoltaics and Earth-abundant catalysts, Science 345 (2014) 1593–1596.

[43] X.L. Ma, X.M. Li, A.D. Jagadale, X.G. Hao, A. Abudula, G.Q. Guan, Fabrication of Cu (OH)₂@NiFe-layered double hydroxide catalyst array for electrochemical water splitting, Int. J. Hydrogen Energy 41 (2016) 14553–14561.

[44] L. Zhou, S. Jiang, Y.K. Liu, M.F. Shao, M. Wei, X. Duan, Ultrathin CoNiP@layered double hydroxides core−shell nanosheets arrays for largely enhanced overall water splitting, ACS Appl. Energy Mater. 1 (2018) 623–631.

[45] J. Liu, J.S. Wang, B. Zhang, Y.J. Ruan, L. Lv, X. Ji, K. Xu, L. Miao, J.J. Jiang, Hierarchical NiCo₂S₄@NiFe LDH heterostructures supported on nickel foam for enhanced overall-water-splitting activity, ACS Appl. Mater. Interfaces 9 (2017) 15364–15372.

[46] Y.F. Zhou, Z.X. Wang, Z.Y. Pan, L. Liu, J.Y. Xi, X.L. Luo, Y. Shen, Exceptional performance of hierarchical Ni–Fe (hydr) oxide@NiCu electrocatalysts for water splitting, Adv. Mater. 30 (2018) 1806769.

[47] S.J. Kim, Y. Lee, D.K. Lee, J.W. Lee, J.K. Kang, Efficient Co–Fe layered double hy-droxide photocatalysts for water oxidation under visible light, J. Mater. Chem. A 2 (2014) 4136–4139.

[48] C. Gong, F. Chen, Q. Yang, K. Luo, F.B. Yao, S.N. Wang, X.L. Wang, J.W. Wu, X.M. Li, D.B. Wang, G.M. Zeng, Heterogeneous activation of peroxymonosulfate by Fe-Co layered doubled hydroxide for efficient catalytic degradation of Rhoadmine B, Chem. Eng. J. 321 (2017) 222–232.

[49] P.S. Li, X.X. Duan, Y. Kuang, Y.P. Li, G.X. Zhang, W. Liu, X.M. Sun, Tuning elec-tronic structure of NiFe layered double hydroxides with vanadium doping toward high efficient electrocatalytic water oxidation, Adv. Energy Mater. 8 (2018) 1703341.

[50] Q.I. Yang, H. Choi, S.R. Al-Abed, D.D. Dionysiou, Iron–cobalt mixed oxide nano-catalysts: heterogeneous peroxymonosulfate activation, cobalt leaching, and fer-romagnetic properties for environmental applications, Appl. Catal. B: Environ. 88 (2009) 462–469.

[51] R.Z. Ma, J.B. Liang, K. Takada, T. Sasaki, Topochemical synthesis of Co-Fe layered double hydroxides at varied Fe/Co ratios: unique intercalation of triiodide and its

profound effect, J. Am. Chem. Soc. 133 (2011) 613–620.

[52] X.W. Teng, D. Black, N.J. Watkins, Y.L. Gao, H. Yang, Platinum-maghemite core-shell nanoparticles using a sequential synthesis, Nano Lett. 3 (2003) 261–264.

[53] L.S. Zhong, J.S. Hu, H.P. Liang, A.M. Cao, W.G. Song, L.J. Wan, Self-assembled 3D flowerlike iron oxide nanostructures and their application in water treatment, Adv. Mater. 18 (2006) 2426–2431.

[54] S.J. Sawhill, K.A. Layman, D.R. Vanwyk, M.H. Engelhard, C.M. Wang, M.E. Bussell, Thiophene hydrodesulfurization over nickel phosphide catalysts: effect of the pre-cursor composition and support, J. Catal. 231 (2005) 300–313.

[55] C. You, Y.Y. Ji, Z.A. Liu, X.L. Xiong, X.P. Sun, Ultrathin CoFe-borate layer coated CoFe-layered double hydroxide nanosheets array: a non-noble-metal 3D catalyst electrode for efficient and durable water oxidation in potassium borate, ACS Sustainable Chem. Eng. 6 (2018) 1527–1531.

[56] L.Z. Zhuang, L. Ge, Y.S. Yang, M.R. Li, Y. Jia, X.D. Yao, Z.H. Zhu, Ultrathin iron-cobalt oxide nanosheets with abundant oxygen vacancies for the oxygen evolution reaction, Adv. Mater. 29 (2017) 1606793.

[57] H.F. Liang, A.N. Gandi, D.H. Anjum, X.B. Wang, U. Schwingenschlögl, H.N. Alshareef, Plasma-assisted synthesis of NiCoP for efficient overall water splitting, Nano Lett. 16 (2016) 7718–7725.

[58] P.F. Liu, S. Yang, B. Zhang, H.G. Yang, Defect-rich ultrathin cobalt-iron layered double hydroxide for electrochemical overall water splitting, ACS Appl. Mater. Interfaces 8 (2016) 34474–34481.

[59] J.T. Ren, G.G. Yuan, C.C. Weng, L. Chen, Z.Y. Yuan, Uniquely integrated Fe-doped Ni(OH)₂ nanosheets for highly efficient oxygen and hydrogen evolution reactions, Nanoscale 10 (2018) 10620–10628.

[60] L. Xu, F.T. Zhang, J.H. Chen, X.Z. Fu, R. Sun, C.P. Wong, Amorphous NiFe nanotube arrays bifunctional electrocatalysts for efficient electrochemical overall water splitting, ACS Appl. Energy Mater. 1 (2018) 1210–1217.

[61] X.G. Wang, W. Li, D.H. Xiong, D.Y. Petrovykh, L.F. Liu, Bifunctional nickel phos-phide nanocatalysts supported on carbon fiber paper for highly efficient and stable overall water splitting, Adv. Funct. Mater. 26 (2016) 4067–4077.

[62] Z. Peng, D.J. Jia, A.M. Al-Enizi, A.A. Elzatahry, G.F. Zheng, From water oxidation to reduction: homologous Ni–Co based nanowires as complementary water splitting electrocatalysts, Adv. Energy Mater. 5 (2015) 1402031.

[63] Y.P. Zhu, T.Y. Ma, M. Jaroniec, S.Z. Qiao, Self-templating synthesis of hollow Co₃O₄ microtube arrays for highly efficient water electrolysis, Angew. Chem. Int. Ed. 56 (2017) 1324–1328.

[64] Y.P. Zhu, Y.P. Liu, T.Z. Ren, Z.Y. Yuan, Self-supported cobalt phosphide mesoporous nanorod arrays: a flexible and bifunctional electrode for highly active electro-catalytic water reduction and oxidation, Adv. Funct. Mater. 25 (2015) 7337–7347.

[65] X.H. Gao, H.X. Zhang, Q.G. Li, X.G. Yu, Z.L. Hong, X.W. Zhang, C.D. Liang, Z. Lin, Hierarchical NiCo₂O₄ hollow microcuboids as bifunctional electrocatalysts for overall water-splitting, Angew. Chem. 128 (2016) 6398–6402.

[66] C. Tang, N.Y. Cheng, Z.H. Pu, W. Xing, X.P. Sun, NiSe nanowire film supported on nickel foam: an efficient and stable 3D bifunctional electrode for full water splitting, Angew. Chem. 127 (2015) 9483–9487.

[67] C.L. Xiao, Y.B. Li, X.Y. Lu, C. Zhao, Bifunctional porous NiFe/NiCo₂O₄/Ni foam electrodes with triple hierarchy and double synergies for efficient whole cell water splitting, Adv. Funct. Mater. 26 (2016) 3515–3523.

[68] H.F. Liang, L.S. Li, F. Meng, L.N. Dang, J.Q. Zhuo, A. Forticaux, Z.C. Wang, S. Jin, Porous two-dimensional nanosheets converted from layered double hydroxides and their applications in electrocatalytic water splitting, Chem. Mat. 27 (2015) 5702–5711.

[69] J.P. Lai, S.P. Li, F.X. Wu, M. Saqib, R. Luque, G.B. Xu, Unprecedented metal-free 3D porous carbonaceous electrodes for full water splitting, Energy Environ. Sci. 9 (2016) 1210–1214.

[70] C.D. Wang, J. Jiang, T. Ding, G.H. Chen, W.J. Xu, Q. Yang, Monodisperse ternary NiCoP nanostructures as a bifunctional electrocatalyst for both hydrogen and oxygen evolution reactions with excellent performance, Adv. Mater. Interfaces 3 (2016) 1500454.

[71] L.A. Stern, L.G. Feng, F. Song, X.L. Hu, Ni₂P as a Janus catalyst for water splitting: the oxygen evolution activity of Ni₂P nanoparticles, Energy Environ. Sci. 8 (2015) 2347–2351.

[72] X. Zhang, H.M. Xu, X.X. Li, Y.Y. Li, T.B. Yang, Y.Y. Liang, Facile synthesis of nickel–iron/nanocarbon hybrids as advanced electrocatalysts for efficient water splitting, ACS Catal. 6 (2016) 580–588.

[73] Y.Q. Sun, K. Xu, Z.X. Wei, H.L. Li, T. Zhang, X.Y. Li, W.P. Cai, J.M. Ma, H.J. Fan, Y. Li, Strong electronic interaction in dual-cation-incorporated NiSe₂ nanosheets with lattice distortion for highly efficient overall water splitting, Adv. Mater. 30 (2018) 1802121.

[74] F.S. Zhang, J.W. Wang, J. Luo, R.R. Liu, Z.M. Zhang, C.T. He, T.B. Lu, Extraction of nickel from NiFe-LDH into Ni₂P@NiFe hydroxide as a bifunctional electrocatalyst for efficient overall water splitting, Chem. Sci. 9 (2018) 1375–1384.

[75] W.J. Liu, J. Bao, M.L. Guan, Y. Zhao, J.B. Lian, J.X. Qiu, L. Xu, Y.P. Huang, J. Qian, H.M. Li, Nickel–cobalt-layered double hydroxide nanosheet arrays on Ni foam as a bifunctional electrocatalyst for overall water splitting, Dalton Trans. 46 (2017) 8372–8376.